Effect of the process atmosphere on glass foam synthesis: A high-temperature environmental scanning electron microscopy (HT-ESEM) study

Francois O. Mear, Renaud Podor, Joseph Lautru, Sébastien Genty, Ronan Lebullenger

Effect of the process atmosphere on glass foam synthesis: a high-temperature environmental scanning electron microscopy (HT-ESEM) study

François O. Méar[a,*], Renaud Podor[b], Joseph Lautru[b], Sébastien Genty [c], Ronan Lebullenger[c]

[a] Univ. Lille, CNRS, Centrale Lille, Univ. Artois, UMR 8181 - UCCS - Unité de Catalyse et Chimie du Solide, F-59000 Lille, France

[b] ICSM, Univ. Montpellier, CNRS, ENSCM, CEA, Marcoule, France

[c] Université de Rennes, CNRS, ISCR-UMR6226, Eq. Verres et Céramiques, F - 35000 Rennes, France

* Corresponding author: francois.mear@univ-lille.fr

Abstract

The effect of the process atmosphere composition on the foam formation of cathode-ray tube (CRT) glass containing graphite and MnO_2 was studied using in situ environmental scanning electron microscopy at high temperature (HT-ESEM). When compared to He+4% H_2, O_2 or air, water steam facilitates glass grain sintering. This is probably due to the formation of hydroxyl groups at the glass grain surface that locally decrease the glass viscosity. We have shown that increasing the steam pressure from 50 Pa to 750 Pa decreases both sintering and foaming onset temperatures by approximately 100°C, favouring the formation of closed pores in viscous glass. At high temperature, the presence of water steam or oxygen promotes foam formation, while the presence of a reducing atmosphere (He+4%H_2) limits glass melt foaming. A synergetic effect of O_2 and H_2O on the onset temperature of glass sintering and foam formation is evidenced.

Keywords: HT-ESEM, CRT glass, MnO_2, Glass-foam, Water steam

1. Introduction

In recent years, there has been very rapid growth in research to define new methods for the recycling of glass cullets from television sets and cathode-ray tube glass in an open loop industry. It involves many problems because of the various waste characteristics, the inhomogeneous composition and the presence of environmentally dangerous elements such as lead, barium and strontium [1]. The most commonly suggested application for CRT glass cullets is in construction industry products [2,3]. The production of foam glass is also a promising method for recycling CRT glass [1]. In general, glass can be transformed into foam by the addition of suitable substances (foaming agents), which generates gaseous products by decomposition or reaction at temperatures above its softening (Littleton) temperature (corresponding to a viscosity of $10^{6.6}$ Pa.s). The interdependence of viscosity and foaming temperature is very sensitive to any change in the chemical composition of the raw materials, especially the type and amount of foaming agent. Several foaming agents (C [4], SiC [5,6], TiN [6], AlN [7], Si_3N_4 [8], glycerol [9], etc.) can be used for silicate-based glass foam formation. Among them, carbon black associated with Mn_3O_4, used as an oxygen releasing agent, contributes to efficient foaming [10,11,12] and yields light glass foams [13,14,15]. To achieve an efficient foaming effect, the foaming agent particles should be trapped in closed pores or embedded in the glass melt. Then, sintering of the glass particles at low temperature is crucial to ensure the closure of porosity, leading to an efficient foaming effect. The glass viscosity and glass particle surface reactivity mainly control the sintering mechanism, and both parameters depend on the glass melt chemistry, i.e., O^{2-} activity and O_2 partial pressure. Furthermore, the presence of water steam in the surrounding atmosphere can lead to the formation of hydroxyl groups at the glass surface, which are active in the glass sintering process.

In the present study, a mixture of graphite and MnO_2 is used as a glass foaming agent. The gradual reduction of MnO_2 into both Mn_2O_3 and Mn_3O_4 during heating under helium flux is reported in the literature [16,17], where the first reduction occurs at 450-600°C (Eq. 1a) and the second occurs before 900°C (Eq. 1b). The decomposition temperatures in an oxidizing atmosphere are very different than those

in a reducing atmosphere, which influences the foaming process, i.e., 627-717°C and T > 900°C, respectively [10].

$$6MnO_{2(s)} \rightarrow 3\ Mn_2O_{3(s)} + 3/2\ O_{2(g)} \quad \text{Eq. 1a}$$

$$3\ Mn_2O_{3(s)} \rightarrow 2\ Mn_3O_{4(s)} + 1/2\ O_{2(g)} \quad \text{Eq. 1b}$$

Manganese can exhibit different oxidation states in oxides [18] and in glass melts [19]. As underlined by Lucktong and Hrma [20], the transition from high to low oxidation forms of transition-metal ions occurs in glass melts at substantially lower temperatures than in pure oxides. Thus, the reaction of Mn_2O_3 with glass can be described as two consecutive mechanisms. The first consists of Mn_2O_3 dissolution in the glass melt (Eq. 2). The second corresponds to the spontaneous reduction of the oxidized species that generates O_2 release (Eq. 3) [21]. Thus, Eq. 3 is the driving reaction for the formation of bubbles in the glass melt and for glass foaming.

$$Mn_2O_3 \rightarrow 2\ Mn^{III}\ (melt) + 3O^{2-}\ (melt) \quad \text{Eq. 2}$$

$$4Mn^{III}\ (melt) + 2O^{2-}\ (melt) \rightarrow 4Mn^{II}\ (melt) + O_2\ (g) \quad \text{Eq. 3}$$

The maximum quantity of Mn dissolved in the glass depends on the solubility of Mn_2O_3 in the glass melt. The foaming reaction that occurs at high temperature is initiated by the reaction between carbon and Mn_2O_3 through complex redox reactions. At the foaming temperature, these reactions depend on the local $P(O_2)$ inside the closed pores that controls the oxidation states of Mn species and their reactivity with carbon black [22,23]. Furthermore, when T > 800°C, the foaming ability is also strongly controlled by the reduction of Mn^{III} cations dissolved in the melt [12]. Consequently, the $P(O_2)$ control in the furnace atmosphere plays an important role in the glass batch process.

In addition, $P(H_2O)$ must be considered an important parameter. Indeed, the presence of water steam induces foaming of glass batches and lowers the formation temperature of the foam [24]. In the production of glass foam, H_2O is recognized as a foaming agent in several ways. First, a common foaming agent is the aqueous solution of Na_2O-SiO_2, also known as “water glass” [25,26]. The majority of H_2O from water glass is

released at 100°C as free water. However, chemically bound OH^- groups form H_2O at higher temperatures, resulting in foaming of the sintered glass [27]. Second, by autoclaving glass powder, H_2O can lead to the formation of an alteration layer at the glass particle surface. By heating the resulting glass/gel, foaming starts to occur at 600°C [28]. In that case, the foaming is caused by the presence of OH groups in the gel layer, which convert into H_2O at high temperatures. Third, the incorporation of water in the glass strongly modifies the glass viscosity: the glass viscosity drops rapidly as the water content increases [29,30,31]. Increasing the water content in glass yields the opening of the glass silica network [29].

Thus, the presence of steam in the surrounding atmosphere has to be considered in the sintering process of the glass. Indeed, the formation of hydroxyl groups can modify the glass surface reactivity and modify the sintering ability, i.e., the formation of closed pores. If the sintering temperature of glass is decreased, then the foaming temperature can also be shifted towards a lower temperature, and the foaming temperature range can be increased.

The aim of the present work is to determine to what extent the partial pressure of H_2O (P_{H2O}) and oxygen pressure (P_{O2}) affect the sintering and foaming ability of a CRT glass mixture composed of 1/3 wt. lead funnel glass + 2/3 wt. panel glass enriched with carbon and MnO_2. To achieve this goal, in situ experiments using a high-temperature environmental scanning electron microscope were performed under various gaseous atmospheres, and the gas pressure in the ESEM chamber was monitored [32].

2. Materials and methods

Sample preparation

Crushed panel and funnel glasses from cathode ray tubes (see Table 1 in Mear et al. [33] for composition) were mixed with 4.4 wt.% MnO_2 (from Merck, 89%) and 0.3 wt.% graphite (from Alfa Aesar, 99.8%, 325 mesh) in a planetary ball mill (Retsch). Then, the powder was uniaxially compressed into a pellet (Ø = 4 mm) at 175 MPa with an initial height of 1 mm.

Heat treatment in HT-ESEM

The pellet was then transferred to a Pt crucible (Ø = 6 mm, height = 3 mm), which was placed in an environmental scanning electron microscope (Quanta 200 ESEM FEG provided by FEI company, Netherlands) equipped with an HT1500 heating stage (FEI company, Netherlands). The sample temperature was measured directly using a Pt-10Rh thermocouple placed below the crucible with an accuracy of ±5°C at 1065°C [34]. The ESEM chamber was first emptied to 10^{-3} Pa, and then gas was added. The samples were heated to 400°C with a 30°C/min heating ramp. At T = 400°C, a thermal shield was placed above the furnace to prevent thermal radiation damage to the gaseous detector device (GDD). The shield was biased with a few tens of volts to attract secondary electrons to the detector and to amplify the electronic signal through the gas [32]. Then, the specimen was heated to 850°C with a 10°C/min heating ramp and held for 30 min. The brightness and contrast were adjusted manually during the heat treatment. The effect of water steam pressure was studied by heat-treating the samples under dry conditions (0.00747 Pa) or wet conditions (50, 200, 400 and 750 Pa H_2O). To identify the effect of the gas nature on the foaming property, several other gases and gas mixtures were also introduced in the ESEM chamber: ambient air (200 and 750 Pa), O_2 (200 Pa) and He+4%H_2 (200 Pa) to determine the effect of P_{O2} in the gas on the foaming efficiency. The images were recorded continuously at 250 times magnification to observe the same region of interest (ROI) and an area sufficiently representative of the whole sample. The relative expansion of the glass foam was estimated by determining the variation in the distance between the objective lens and the sample surface (working distance).

Complementary analyses (back-scattered electron images and EDS analyses) were performed using ESEM in high-vacuum mode after cooling the sample to room temperature.

Heat treatment in heating microscope

The heating microscope was equipped with a blue LED lamp, and images were recorded using a CCD black and white camera with a telocentric lens with a resolution of 30 µm/pixel. The thermal lag between the

sample and the thermocouple located below the sample was determined by comparing the measured temperatures with the melting or decomposition temperature of Zn (99.999%, Sigma-Aldrich, St. Louis, MO, $T_{melting}$ = 419.5°C), Al (99.999%, Sigma-Aldrich, $T_{melting}$ = 660°C), $BaCO_3$ (99.999%, Sigma-Aldrich, $T_{melting}$ = 811°C), Ag (99.99%, Sigma-Aldrich, $T_{melting}$ = 961.8°C), and Au (99.99%, Sigma-Aldrich, $T_{melting}$ = 1063°C). The sample was heated with a 10°C/min ramp and held for 30 min at T = 850°C.

Image analysis of sintering and foaming of glass

The glass sintering and glass foaming were determined by measuring the distance between two particles along the image series. The position of these particles was determined by image processing using the TrackMate particle tracking plugin [35] of ImageJ software [36]. The nearest distance (*L*) between the selected particles was calculated by using the coordinates (*x*,*y*) of two particles (Eq. 4):

$$L = \sqrt{(x_1 - x_2)^2 + (y_1 - y_2)^2} \quad \text{Eq.4}$$

The distance *L* was then normalized to the distance found at approximately 50 - 75°C (L_0). Thus, L/L_0 values were plotted as a function of temperature, and the curves were used to characterize the glass pellet behaviour as a function of the temperature.

3. Results and discussion

Description of the general behaviour of foam glass formation

The series of images that were recorded by HT-ESEM for each sample are presented as movies (see Supplementary Files S1 to S9). From these images, morphological information regarding the *x* and *y* directions was extracted using image processing, allowing precise quantification of the sample sintering and foaming.

The sample deformation in the *z* direction was determined using the working distance. Indeed, the *z*-position of the platinum crucible in which the sample is located remains constant during the experiment. Thus, the variation of the working distance during the heat treatment will only correspond to the sample

expansion (i.e., foaming) in the *z*-direction. Moreover, although we cannot be sure that the observed area is the highest in the sample during foam formation, for the sake of simplification, we will assume that the sample foaming observed in the *z*-direction of the ROI is representative of the complete sample. For all samples, the observed foaming between the beginning and the end of the experiment ranges between 20 and 130%.

The sample inserted in the ESEM chamber consists of particles that are in contact. Their size ranges between a few micrometres to approximately 100 µm. From the image series, several consecutive transformations are systematically observed, as reported in Figure 1. The corresponding temperature ranges can be determined from the modifications that occur at the microscopic scale.

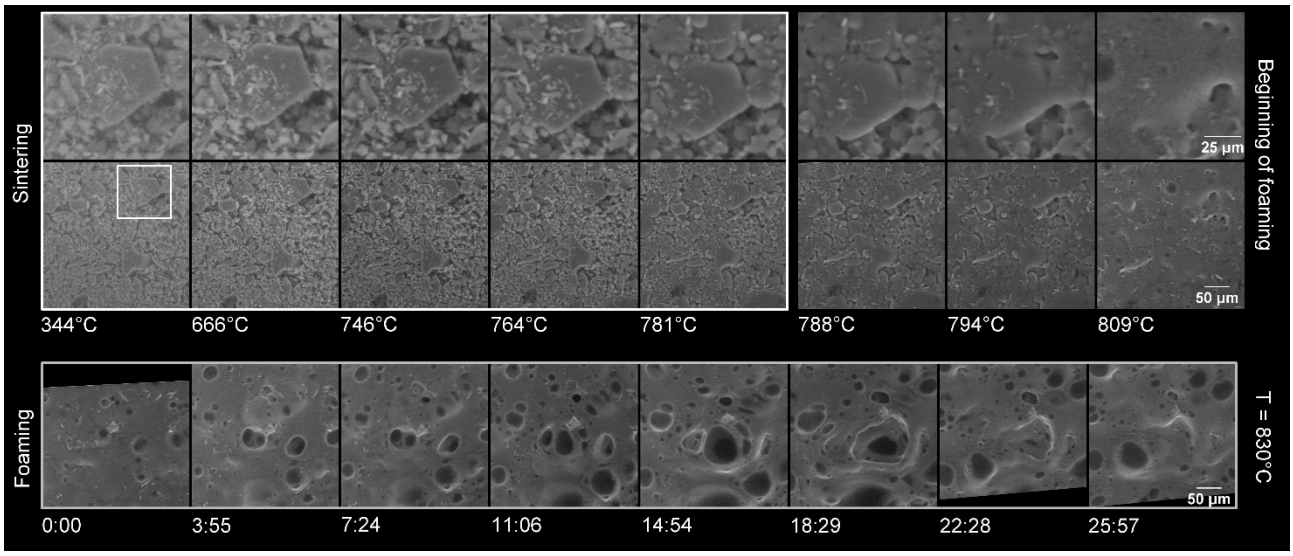

Figure 1. Morphological modifications observed on a "CRT glass + 4.4 wt.% MnO_2 + 0.3 wt.% C" sample during the in situ formation of glass foam in ESEM using a 750 Pa water vapour atmosphere. Sintering is efficient in the low temperature domain (from room temperature to 787°C) identified by the images marked with a white rectangle. Foam formation begins at 788°C. Intense foaming (with bubble formation and outgassing) is observed when T is equal to 830°C under these conditions. The images are marked with a grey rectangle. Note that the first line of images is a magnified view of the top right zone of the second line of images, marked by a white square in the image recorded at T = 344°C.

The morphological modifications of the glass generally occur according to the following steps (under 750 Pa air, see Figure 1):

- At T ~ 430°C, limited movements of small particles can be observed from place to place. This can correspond to the oxidation of a part of the carbon particles into CO and/or CO_2 by oxidizing gases (O_2, steam). These particles remain observable until the end of the experiment, meaning that they are not fully oxidized.
- At a higher temperature (T = 750°C), sphering of the glass particles is observed. This change in the glass grain shapes indicates that the softening point of the glass is reached.
    - Then, the grains begin to stick to each other, leading to the sintering of the glass grains. At this stage, the smallest glass particles merge completely with the largest ones: sintering of the glass particles occurs.
- The sintering of particles accelerates up to the complete closure of the surface porosity of the sample. The corresponding temperature ranges between 780 and 790°C.
- From T = 788°C onwards, the details observable in the images start to diverge from each other, highlighting the start of foaming of the sample. At this stage, pores or bubbles are not detected.
- While increasing the temperature and/or continuing the heating of the sample, large pores and bubbles are formed at the surface of the sample, and glass foam formation is directly observed.

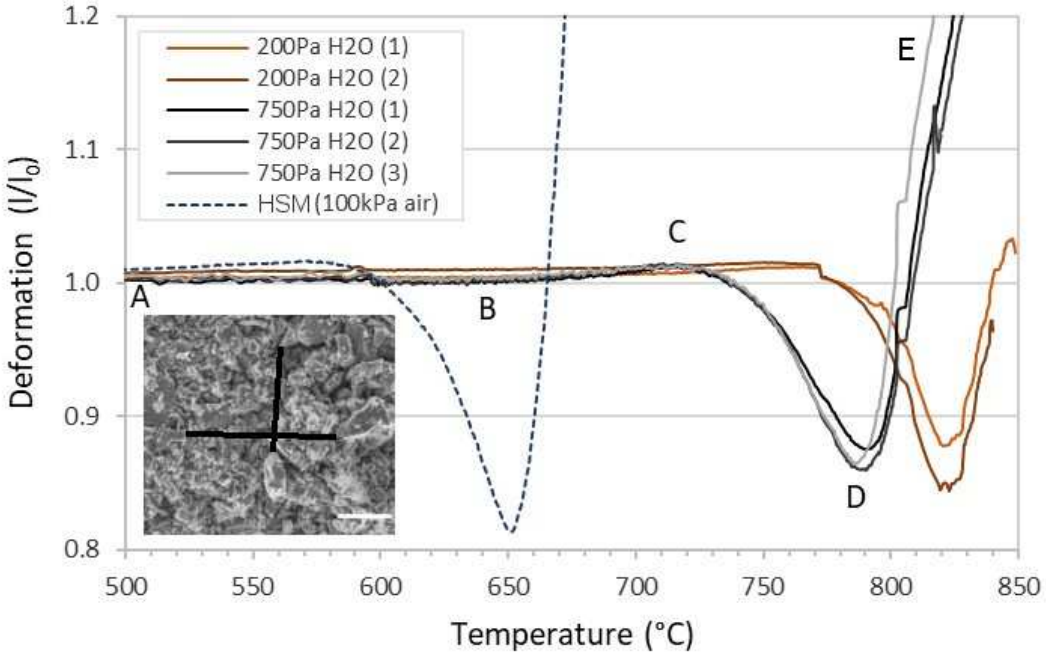

Figure 2. Sample length variations determined from the HT-ESEM image series (the hot-stage microscopy (HSM) curve recorded in air at 1 atm is reported for comparison). Feature points A, B, C, D and E are related to the 750 Pa H_2O curves. The inserted image shows the detection of the points of interest (the white scale bar corresponds to 100 µm).

When looking at a particular image series, one can observe that the different stages of the sample transformation reported previously correspond to the displacement of small particles towards each other. The positions of several points of interest were tracked from the beginning to the end of the experiment, and the distances between those points were determined (insert in Figure 2). When reporting these data as a function of temperature, the curves that are obtained (Figure 2) can be used to characterize the sample behaviour during the heat treatment. Indeed, the sample behaviour can be related to the previous description of the sample modifications at the microscopic scale, i.e., no modification of the sample size (A to B), limited dilatation of the sample (B to C), sintering of the sample (C to D) and foaming of the sample (D to E). Foaming, observed at a high temperature, is characterized on this curve by irregularities in the expansion of the sample between D and E, when the displacement of the points of interest becomes erratic

with the formation, expansion and breaking of the gas bubbles (Figure 1). The breaking of the gas bubbles is characterized by self-healing of the glass at the location where the gas was released.

A curve determined from hot-stage microscopy (HSM) measurements in ambient air is reported in Figure 2 for comparison. The temperature shift observed between both sets of measurements could be attributed to the difference in the surrounding atmosphere compositions (air at a 100 kPa pressure for HSM and 200/700 Pa water vapour for curves derived from the HT-ESEM data). However, the general shape of the HSM curve (A) is close to the data obtained from the HT-ESEM image series, but the characteristic temperatures (e.g., sintering temperature) are shifted to lower values. This finding clearly indicates that the sample deformation in the *x*,*y* plane (observed with HT-ESEM) is similar to what is classically observed in the *x*,*z* or *y*,*z* plane (observed by HSM).

To compare the effect of the nature of the atmosphere surrounding the sample (composition and pressure) on the glass behaviour, two main parameters were determined from these curves: (i) the sintering temperature (T_s), which corresponds to the temperature value at which -0.4% of the sintering of the sample is observed, and (ii) the foaming temperature (T_{foam}), which is equivalent to the onset of foaming ($T_{f,onset}$) measured at the inversion point observed on the curve between sintering and foaming.

The percentage of vertical foaming of the sample ($\%V_{foam}$) is estimated by comparing the working distance determined at the beginning of the experiment (WD_{begin}) with the working distance determined at a temperature value of $T = T_{foam} + 50°C$ (WD_{TF+50}) and at the end of the experiment (WD_{end}). The initial height of the sample h is 1 mm. It is determined according to Eq. 5:

$$\%V_{foam} = 100 \times (h + (WD_{begin} - WD_{TF+50})/h) \qquad \text{Eq. 5}$$

Several experiments have been performed using different types of gases and gas pressures. The operational values and characteristic parameters determined from these experiments are gathered in Table 1.

When foaming is observed, the formation of large bubbles at the surface of the sample that grow and explode generates important displacements of the points of interest. Then, the position of these points

becomes erratic. As a consequence, their relative displacements cannot be directly correlated with the general behaviour of the glass (i.e., growth of the sample due to the formation of gas bubbles). Thus, these data will not be used to characterize the sample deformations.

Table 1. Summary of the data related to the glass foam formation experiments. When the experiments were performed with air, the temperature of air in the ESEM room was 24°C, and its relative humidity was 50%. Two values are reported for vertical foaming. The first one is measured when the sample temperature is equal to T_{foam}+50°C (30°C), and the second one is measured at the end of the experiment.

Gas	P_{tot} (Pa)	P_{O2} (Pa)	P_{H2O} (Pa)	T_s (°C)	T_{foam} (°C)	Vertical Foaming (%)	Remarks
He+4%H_2	200	0	0	825	918	20 - 40	End of exp --> H_2O is injected
H_2O	50	0	50	836	910	40 - 40	At T=T_{foam}+30°C / end of exp
H_2O	200	0	200	777	819	50 - 130	At T=T_{foam}+50°C / end of exp
H_2O	400	0	400	750	809	60 - 90	At T=T_{foam}+50°C / end of exp
H_2O	750	0	750	718	789	80 - 90	At T=T_{foam}+50°C / end of exp
air	200	42	3	793	906	30 - 110	At T=T_{foam}+50°C / end of exp
air	750	157	11	764	809	40 - 80	At T=T_{foam}+50°C / end of exp
O_2	200	200	0	788	870	80 - 130	At T=T_{foam}+50°C / end of exp
Vacuum	-	-	-	811	882	30 - 30	At T=T_{foam}+50°C / end of exp

Foaming in a reducing atmosphere

The formation of glass foam was studied under 200 Pa He + 4% H_2, i.e., under a non-oxidizing and dry atmosphere. Sintering begins at 825°C, and foaming occurs at 918°C. The temperature for the beginning of glass sintering is the highest value determined among the experiments that were performed during this study. Under these conditions, as no water or oxygen is present in the reactive media, no particular species are formed at the surface of the glass particles. Then, glass particle coarsening is not enhanced, and the sintering temperature value is high. In a 200 Pa He + 4% H_2 atmosphere, the foaming agents present different behaviours. The carbon is not oxidized (no movement of the carbon particles is observed at T = 430°C), and it probably does not participate directly in the formation of gaseous species or glass foaming. In

parallel, at high temperatures (800-1000°C) and under a reducing atmosphere, the Mn^{III} species are partially reduced into Mn^{II} species with a subsequent release of O_2 gas (Eq. 3). These species participate in limited oxidation of the carbon particles that are trapped in the pores and generate limited foaming of the glass pellet at high temperatures. Under these conditions, the formation of bubbles is less intense than under other conditions. The percentage of vertical foaming that is measured is approximately 20% of the initial height of the sample, indicating that foaming remains limited in these conditions.

Foaming in an oxidizing atmosphere

The formation of glass foam was also studied under 200 Pa pure O_2 pressure, i.e., an oxidizing and dry atmosphere. Under these conditions, Mn_2O_3 is stable up to the end of the experiment, and all Mn^{III} available can be incorporated in the glass melt (Eq. 2) and contributes to the generation of O_2 according to Eq. 3. The sintering and foaming temperatures are 788°C and 870°C, respectively. The decrease in the characteristic temperatures compared to the values determined under reducing (and dry) conditions is approximately 50°C. This is due to the change in the manganese chemistry in the glass melt. The modification of the oxidation degree of Mn, the variations in the ratio of stable Mn^{III} and Mn^{II} species in the glass and the increase in the total amount of Mn in the glass melt can modify the glass melt properties, particularly the melt viscosity below 800°C [37]. Both a decrease in the glass melt viscosity under oxidizing conditions due to the increase in the total amount of manganese in the glass and an increase in the Mn^{III}/Mn^{II} ratio facilitate glass particle sintering at lower temperatures.

The percentage of vertical swelling measured at $T_{foam+50}$ was 80% (and was equal to 130% at the end of the experiment). This value is much higher than the value determined when using a reducing atmosphere. This value implies that many bubbles are formed during the heat treatment, i.e., a significant amount of oxygen is released according to Eq. 3. This is in good agreement with the findings of Lucktong and Hmra [20]. Furthermore, in the presence of pure oxygen, all carbon is oxidized to CO and/or CO_2, and a higher quantity of gases will be produced, leading to substantial foaming at the end of the experiment.

Foaming in a humid atmosphere

Experiments of glass foam formation were performed under pressure values ranging from 50 to 750 Pa H_2O. The oxygen content in the gas is relatively low, as the oxygen partial pressure in steam is on the order of 10^{-3} Pa O_2 in 200 Pa H_2O (the steam is generated from a water bottle that is heated at T = 30°C). Under these conditions, Mn_2O_3 will remain stable up to 900°C. The different characteristic temperatures are gathered in Table 1 and reported in Figure 3. Both sintering and foaming temperatures decrease as the steam pressure increases in the ESEM chamber.

Concerning the sintering process, the effect of water vapour on glass sintering is poorly documented in the literature [38]. The main hypothesis to explain the effect observed in the present study is that the water molecules adsorbed on the surface of the grains modify the Si-O bond energies by reducing the energy required (and thus the temperature) for the formation of intergrain bonds. When glass melts contain water, their viscosity is lower than that of the corresponding anhydrous glass melt [30,31,39]. Thus, in the presence of moisture, the surface viscosity of the grains decreases, favouring the coalescence of glass grains at lower temperatures. Such an effect has been evidenced at medium temperatures for glass healing in the presence of water in the healing atmosphere [40]. Girard et al. indicated that the viscosity of the glass surrounding cracks can be significantly reduced by water diffusion and glass hydrolysis at T = 620°C. Thus, if glass melt viscosity decreases with increasing water gas pressure, the sintering temperature will also decrease as the steam pressure will increase.

The variations in the foaming temperatures are similar to those observed for the sintering temperatures. Even if the chemistry of Mn in the glass melt can be slightly modified in terms of the Mn^{III}/Mn^{II} ratio, the quantity of O_2 release in each water pressure condition should not vary drastically between 50 and 750 Pa. Similarly, the quantity of gases released due to carbon oxidation will not vary depending on the steam pressure in the explored pressure range. Then, the foaming temperatures are probably directly related to

the glass melt viscosity: all the glass melts present the same behaviour but with a temperature shift due to the differences in the glass melt viscosities.

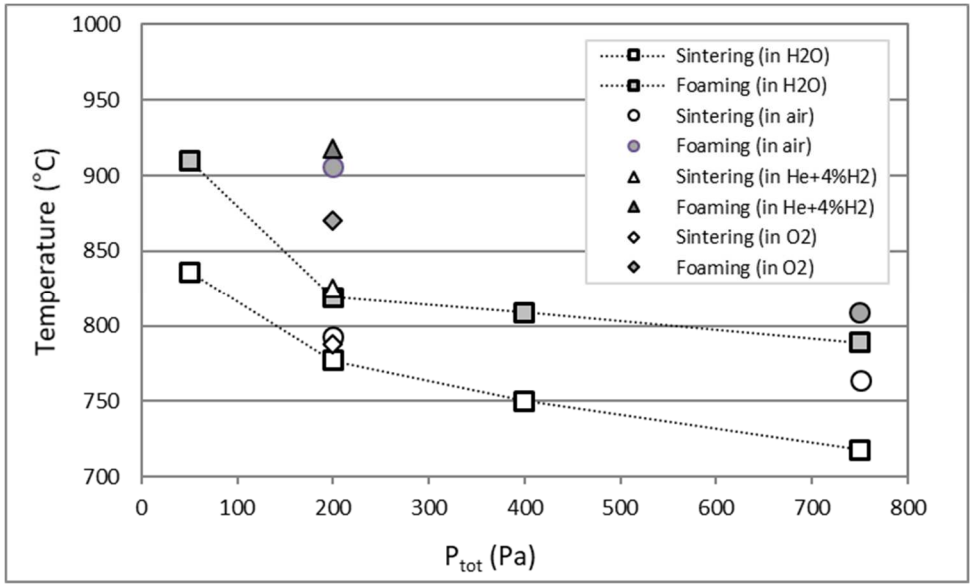

Figure 3. Variation of the sintering temperature (T_s measured at -0.4% sintering) and the foaming temperature (T_{foam} measured at the inversion point between sintering and foaming) for a mixture composition of CRT glass + 4.4 wt.% MnO_2 + 0.3 wt.% C.

Foaming in an air atmosphere

Two experiments were performed under an air atmosphere at different pressure values. The gas should be considered a gas mixture containing 21% O_2 and 0.2% H_2O (T = 24°C and relative humidity = 50% in the experimental conditions). Then, these conditions can combine the effects of an oxidizing atmosphere and a low water vapour pressure (a few Pa) atmosphere.

One experiment was performed under 200 Pa air. The total pressure corresponds to relative pressures P_{O2} = 42 Pa and P_{H2O} = 3 Pa. The T_S and T_{foam} values that have been measured are 793°C and 906°C, respectively. These values are intermediate between those determined for 50 Pa H_2O and 200 Pa O_2 (see Table 1), indicating the accumulative effect of each gas.

A second experiment was performed under 750 Pa air (corresponding to partial pressures of oxygen and water such as P_{O2} = 157 Pa and P_{H2O} = 11 Pa). The T_s and T_{foam} values determined under 750 Pa air are 764°C and 809°C, respectively. Both values are lower than those determined when the experiment was performed under 200 Pa pure O_2 or with 50 Pa water vapour. Thus, the presence of both oxygen and water vapour in the atmosphere surrounding the sample tends to lower the T_s and T_{foam} values to a larger extent than the effect of each gas considered separately. In this case, a synergetic effect of the presence of both O_2 and H_2O gases in the atmosphere is observed. The presence of O_2 probably increases the total content of Mn^{III} + Mn^{II} species dissolved in the glass melt, as already reported for chromium species dissolved in glass melts [41,42]. This parameter lowers the glass melt viscosity, as the presence of water vapour in the gas also does. The decrease in the glass melt viscosity corresponds to a decrease in the T_s and T_{foam} values.

Furthermore, the vertical height swelling at the end of the experiment is 110% and 80% for 200 and 750 Pa air, respectively. Under these experimental conditions, Mn_2O_3 is the stable manganese oxide in equilibrium with the glass melt. During the partial dissolution of Mn_2O_3 in the glass melt and the equilibration of the dissolved species with the melt, a limited quantity of Mn species is reduced into Mn^{II} species. This reduction is associated with a release of a limited quantity of gas under the experimental conditions that is probably not enough to form bubbles. However, during these two experiments, all of the carbon can be oxidized into CO and/or CO_2 by oxygen that is present in the air, yielding an important release of gases that generates the foaming of the glass.

Foaming agent particles

The foaming agent particles cannot be easily distinguished from the rest of the sample since the images are secondary electron images and are recorded at relatively low magnification (Figure 4). First, the active foaming agent particles, which will release gases during the high-temperature reaction, are enclosed in the closed pores present inside the sample (because the gases generated by these particles should be trapped into the sample to be efficient in forming the foam). Then, it is impossible to observe them directly. Second,

some particles that are not pieces of glass are observed from the beginning to the end of the experiment, as they remain as supernatants at the glass melt surface (Figures 4a to 4d – one particle is shown at the end of the arrow). These particles are carbon particles floating on the glass melt. These particles were also observed using BSE imaging after sample cooling (Figures 4e & 4f).

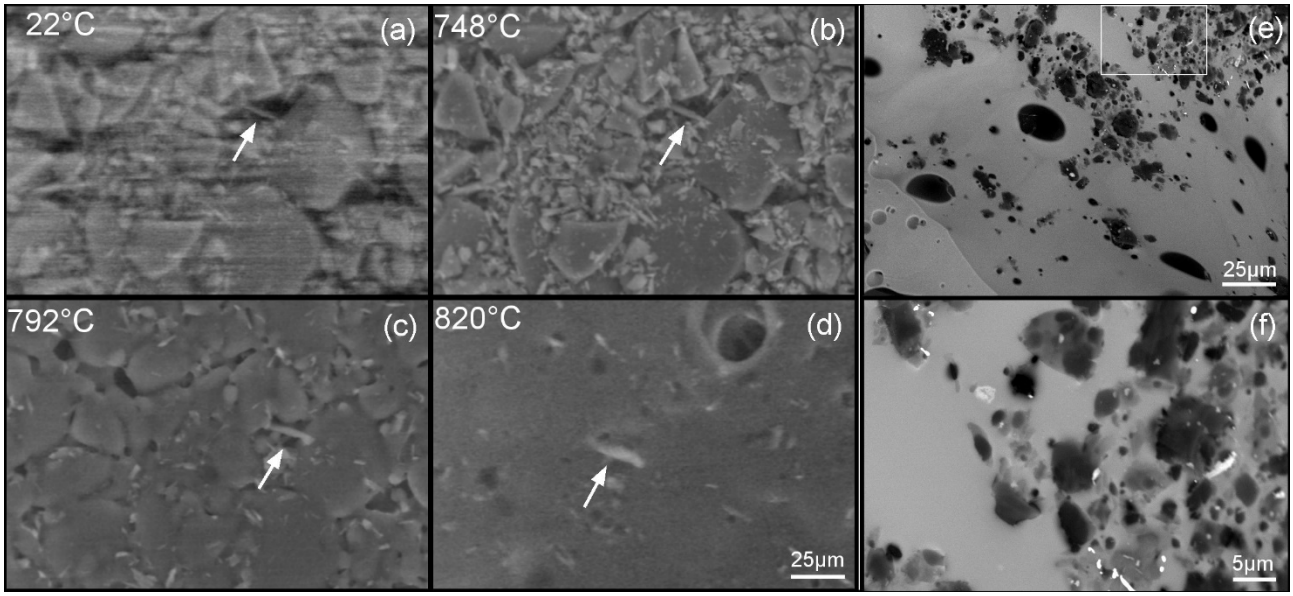

Figure 4. "CRT + 4.4 wt.% MnO_2+ 0.3 wt.% C" glass foam formation. **(a - d)** In situ experiment showing a carbon particle (indicated by the white arrow) during the heat treatment from RT to 820°C. **(e)** Backscattered electron (BSE) image recorded after sample cooling to RT showing the distribution of the carbon particles (in black) at the foam surface. **(f)** Enlarged view of the white square in (b).

4. Discussion

The presence of water steam in the gas surrounding the sample during heating modifies the shrinkage mechanism of the glass grains. When steam is in contact with the glass surface, hydroxyl groups form, and the glass viscosity decreases. Thus, the shrinkage temperature of the glass pellet decreases as the water pressure in the gas increases. The temperature decrease is higher than 120°C when the steam pressure increases from 50 Pa to 750 Pa. When compared to the effect of the other gases used in the present study

(experiments performed at 200 Pa under various gases), water vapour is the most efficient gas to enhance the sintering of glass grains.

When the sample heating is continued, foam begins to form. The shift of the sintering temperature to lower values facilitates the formation of closed pores in which the foaming agents are trapped. Thus, the foaming onset temperature also decreases with increasing steam pressure. At high temperatures, foaming is controlled by complex redox reactions [12]. However, the presence of neutral (water vapour) or oxidizing (air, O_2) gases seems to promote foam formation, while reductive gases (mixture of He + 4% H_2) seem to inhibit foam formation. This is probably due to the nature of the Mn oxides as well as the oxidation state of Mn dissolved in the glass melt. Indeed, if the manganese species are mainly in valence state II, then they will not react with carbon to form CO and/or CO_2 gases. Thus, foaming remains limited. It is clear that the redox reactions and the nature of the species that are formed in the glass melt by the foaming agents are crucial during glass foam formation (gas formation, variation in glass melt viscosity, etc.).

The presence of both oxygen and water vapour in the gas surrounding the sample has a synergetic effect that yields a decrease in the glass sintering temperature and the foaming temperature. On the one hand, oxygen leads to the oxidation of carbon particles. On the other hand, water vapour yields a decrease in the glass sintering temperature (as it decreases the glass viscosity). Thus, the temperature for the formation of the first glass bubbles is decreased, and these bubbles can grow easily as carbon particles are trapped with oxygen in closed pores. Therefore, the effect of two gases on foam formation can be more efficient than the effect of each gas considered separately. Recently, Hribar et al. [43] showed that the addition of water glass (i.e., Na_2O-$xSiO_2$ glass) to CRT panel glass can yield a decrease in the sintering and foaming temperatures, as well as an increase in foam formation, when the sample is heated in air. These observations are consistent with those reported in the present study.

5. Conclusions

In this study, the effect of the nature of the process atmosphere (reducing, oxidizing, steam and wet air) on the characteristic temperatures of glass foam formation using in situ high-temperature environmental scanning electron microscopy was determined.

The partial pressure of H_2O affects the sintering and the foaming ability as increasing the P_{H2O} shifts the sintering and foaming temperatures to lower values. The presence of H_2O affects the glass particle surfaces, as it modifies the viscosity of the glass melt. Under reducing (He + 4% H_2) and oxidizing (O_2) atmospheres, the main changes that have been measured can be attributed to the reactivity of the foaming agents in terms of the nature of the gas as well as the complex reactions and competition between the dissolution of Mn_2O_3 and redox equilibrium of Mn^{III} and Mn^{II} species in the glass melt.

Cumulative and synergetic effects of different gases, mainly wet air containing oxygen and water vapour, on the foaming efficiency have been evidenced. These findings could be used as guidelines for the choice of the atmosphere during glass foam production and saving energy at lower processing temperatures.

Acknowledgements

We are grateful to the RecyverProject (Univ. Rennes, Univ. Lille, Ecosystèmes, 2013-2015) for funding the research and Environnement Recycling for supplying the CRT glasses.

References

[1] F. Méar, P. Yot, M. Cambon, M. Ribes, Elaboration and characterisation of foam glass from cathode ray tubes, Adv. Appl. Ceram.: Structural, Functional and Bioceramics, 104 (3) (2005) 123-130,https://doi.org/10.1179/174367605X20171

[2]L. Jiang, K. Onitsuka, Construction utilization of foamed waste glass, J. Environ. Sci., 16 (2004) 302-307

[3] G. Betti, U. Pinori, A. Marradi, The use of recycled glassfoam aggregates for lightweight embankment. M. Losa, T. Papagiannakis (Eds.), Sustain. Eco-Efficiency, Conserv. Transp. Infrastruct. Asset Manag., CRC Press (2014) 245-254

[4] J.M. Kirkpatrick, Process for Making a Cellulated Vitreous Material, US Patent, 4 (1978) p.224, 198

[5] G.A. Blengini, M. Busto, M. Fantoni, D. Fino, Eco-efficient waste glass recycling: integrated waste management and green product development through LCA, Waste Manag. 32 (2012) 1000-1008, https://doi.org/10.1016/j.wasman.2011.10.018

[6] F. Mear, P. Yot, M. Cambon, M. Ribes, The changes in lead silicate glasses induced by the addition of a reducing agent (TiN or SiC), J. Non-Cryst. Solids 351 (2005) 3314-3319, https://doi.org/10.1016/j.jnoncrysol.2005.08.019

[7] R. Lebullenger; S. Chenu; J. Rocherullé; O. Merdrignac-Conanec; F. Cheviré; F. Tessier; A. Bouzaza; S. Brosillon, Glass foams for environmental applications, J. Non-Cryst. Solids 356 (2010) 2562-2568, https://doi.org/10.1016/j.jnoncrysol.2010.04.050

[8] J. García-Ten, A. Saburit, M. J. Orts, Glass foams from oxidation/reduction reactions using SiC, Si_3N_4 and AlN powders, Glass Technol.: Eur. J. Glass Sci. Technol. A 52 (2011) 103-110, https://www.ingentaconnect.com/content/sgt/gta/2011/00000052/00000004/art00001

[9] J.V. Valentovich, R.S. Borisovich, R.S. Sergejevich, Granulated Foam Silicate (Penostek) Production Method (2009). World patent 2011/027194 A1

[10] R.R. Petersen, J. König, Y. Yue. The mechanism of foaming and thermal conductivity of glasses foamed with MnO_2, J. Non-Cryst. Solids, 425 (2015) 74-82, https://doi.org/10.1016/j.jnoncrysol.2015.05.030

[11] J. König, R.R. Petersen, Y. Yue, D. Suvorov, Gas-releasing reactions in foam-glass formation using carbon and Mn_xO_y as the foaming agents, Ceram. Int. 43 (2017) 4638-4646, https://doi.org/10.1016/j.ceramint.2016.12.133

[12] R. R. Petersen, J. König, N. Iversen, M. B. Østergaard, Y. Yue, The foaming mechanism of glass foams prepared from the mixture of Mn_3O_4, carbon and CRT panel glass, Ceram. Int. 47 (2021) 2839-2847,https://doi.org/10.1016/j.ceramint.2020.09.138

[13] M.B. Østergaard, R.R. Petersen, J. König, Y. Yue, Effect of alkali phosphate content on foaming of CRT panel glass using Mn_3O_4 and carbon as foaming agents, J. Non-Cryst. Solids 482 (2018) 217-222, https://doi.org/10.1016/j.jnoncrysol.2017.12.041

[14] M.B. Østergaard, B. Cai, R.R. Petersen, J. König, P.D. Lee, Y. Yue, Impact of pore structure on the thermal conductivity of glass foams, Mater. Lett., 250 (2019) 72-74, https://doi.org/10.1016/j.matlet.2019.04.106

[15] J. König, A. Lopez-Gil, P. Cimavilla-Roman, M.A. Rodriguez-Perez, R.R. Petersen, M.B. Østergaard, N. Iversen, Y. Yue, M. Spreitzer, Synthesis and properties of open- and closed-porous foamed glass with a low density, Construct. Build. Mater. 247 (2020) 118574, https://doi.org/10.1016/j.conbuildmat.2020.118574

[16]W.M. Dose, S.W. Donne, Kinetic analysis of c-MnO_2 thermal treatment, J. Therm. Anal. Calorim. 105 (2011) 113-122, https://doi.org/10.1007/s10973-011-1445-5

[17] K. Terayama, M. Ikeda, Study on Thermal Decomposition of MnO_2 and Mn_2O_3 by Thermal Analysis, Trans. Jpn. Inst. Met. 24 (1983) 754-758, https://www.jstage.jst.go.jp/article/matertrans1960/24/11/24_11_754/_pdf/-char/ja

[18] J.E. Post, Manganese oxide minerals: crystal structures and economic and environmental significance, Proc. Natl. Acad. Sci. U. S. A, 96 (1999) 3447-3454, https://doi.org/10.1073/pnas.96.7.3447

[19] W. Thiemsorn, K. Keowkamnerd, S. Phanichphant, P. Suwannathada, H. Hessenkemper, Influence of Glass Basicity on Redox Interactions of Iron–Manganese–Copper Ion Pairs in Soda–Lime–Silica Glass, Glass Phys. Chem. 34 (1)(2008) 19-29, link.springer.com/article/10.1134/S1087659608010033

[20] C. Lucktong, P. Hrma, Oxygen Evolution During MnO-Mn_3O_4 Dissolution in a Borosilicate Melt, J. Am. Ceram. Soc., 71 (5) (1988)323-28, https://doi.org/10.1111/j.1151-2916.1988.tb05048.x

[21] A. Paul, R.W. Douglas, Mutual Interaction of Different Redox Pairs in Glass, Phys. Chem. Glasses, 7 [l] (1966) 1-13

[22] F.E. Şeşen, Practical reduction of manganese oxide, J. Chem. Tech. App. 1(1) (2017) 1-2, 10.35841/chemical-technology.1.1.26-27

[23] S.E. Olsen, S. Olsen, M. Tangstad, Production of manganese ferroalloys, Tapir Academic Press, Trondheim, Norway. 2007.

[24]P.R. Laimböck, Foaming of glass melts. PhD thesis, Technische Universiteit Eindhoven (1998) 261pp. https://doi.org/10.6100/IR511210

[25] D. Hesky, C. G. Aneziris, U. Groß, A. Horn, Water and waterglass mixtures for foam glass production, Ceram. Int. 41 (10) (2015) 12604-12613, https://doi.org/10.1016/j.ceramint.2015.06.088

[26]T. Elmer, Porous and Reconstructed Glasses, Engineered Materials Handbook, Vol 4, Ceramic and Glasses, p 427-32, copyright 1932, ASM International, Materials Park, OH 44073-0002.

[27] I. Vaisman, A. Ketov, I. Ketov, Cellular glass obtained from non-powder preforms by foaming with steam, Ceram. Int. 42 (2016) 15261–15268, https://doi.org/10.1016/j.ceramint.2016.06.165

[28] M. Suzuki, S. Maruyama, N. Umesaki, T. Tanaka, Hydroxyl-Group Identification Using O K-Edge XAFS in Porous Glass Fabricated by Hydrothermal Reaction and Low-Temperature Foaming, Molecules 24(19) (2019) 3488, https://doi.org/10.3390/molecules24193488

[29]R.R. Barthelemew, High-water containing glasses, J. Non Cryst. Solids 56 (1983) 331-342,https://doi.org/10.1016/0022-3093(83)90490-8

[30] P. Del Gaudio, H. Behrens, J. Deubener, Viscosity and glass transition temperature of hydrous float glass, J. Non Cryst. Solids 353 (2007) 223–236, https://doi.org/10.1016/j.jnoncrysol.2006.11.009

[31] J. Deubener, H. Behrens, R. Müller, S. Zietka, S. Reinsch, Kinetic fragility of hydrous soda-lime-silica glasses, J. Non Cryst. Solids 354 (2008) 4713–4718, https://doi.org/10.1016/j.jnoncrysol.2008.04.021

[32] R. Podor, G.I. Nkou Bouala, J. Ravaux, J. Lautru, N. Clavier, Working with the ESEM at high temperature, Mater. Charact. 151 (2019) 15-26, https://doi.org/10.1016/j.matchar.2019.02.036

[33] F. Mear, P. Yot, M. Cambon, M. Ribes, The characterization of waste cathode-ray tube glass, Waste Manage. 26 (2006) 1468–1476, https://doi.org/10.1016/j.wasman.2005.11.017

[34]R. Podor, D. Pailhon, J. Ravaux, H.P. Brau, Development of an Integrated Thermocouple for the Accurate Sample Temperature Measurement during High Temperature Environmental Scanning Electron Microscopy (HT-ESEM) Experiments, Microsc. Microanal. 21(2) (2014) 307-312, https://doi.org/10.1017/S1431927615000252

[35]J.Y.Tinevez, N. Perry, J. Schindelin, G.M.Hoopes, G.D. Reynolds, E. Laplantine, S.Y.Bednarek, S.L.Shorte, K.W. Eliceiri,TrackMate: An open and extensible platform for single-particle tracking, Methods 115 (2017) 80-90, https://doi.org/10.1016/j.ymeth.2016.09.016

[36]C.A.Schneider, W.S. Rasband, K.W. Eliceiri, NIH Image to ImageJ: 25 years of image analysis, Nat. Methods 9 (2012) 671-675,

[37] G. Scarinci, G. Brusatin, E. Bernardo, Glass foams, in M. Scheffler, P. Colombo (Eds.), Cell. Ceram. Struct. Manuf. Prop. Appl., Wiley-VCH Verlag (2005), pp. 158-176

[38] I. B. Cutler, Effect of water vapor on the sintering of glass powder compacts. J. Am. Ceram Soc. 52 (1969) 11-13, https://doi.org/10.1111/j.1151-2916.1969.tb12651.x

[39]H. Ni, H. Hui, G. Steinle-Neumann, Transport properties of silicate melts, Rev. Geophys.53 (2015) 715-744, https://doi.org/10.1002/2015RG000485

[40] R. Girard, A. Faivre, F. Despetis, Influence of Water on Crack Self-Healing in Soda-Lime Silicate Glass, J. Am. Ceram. Soc. 94 (8) (2011) 2402–2407, https://doi.org/10.1111/j.1551-2916.2011.04517.x

[41] H. Khedim, R. Podor, C. Rapin, M. Vilasi, Redox-Control Solubility of Chromium Oxide in Soda-Silicate Melts. J. Am. Ceram. Soc., 91 (11) (2008) 3571–3579, https://doi.org/10.1111/j.1551-2916.2008.02692.x

[42] V. Szczepan, F. Brix, C. Petitjean, P.J. Panteix, M. Vilasi, A new modeling of the dissolution of chromia in Na_2O-SiO_2 liquids. J. Non-Cryst. Sol. (545) (2020) 120153, https://doi.org/10.1016/j.jnoncrysol.2020.120153

[43]U. Hribar, M. Spreitzer, J. König, Applicability of water glass for the transfer of the glass-foaming process from controlled to air atmosphere. J. Clean. Prod. 282 (2021) 125428, https://doi.org/10.1016/j.jclepro.2020.125428